0.75 mm and an increment of 0.4 mm. A field of view of 180 × 180 mm^2, 512 × 512 matrix, and medium smooth convolution kernel (B25f) were applied. The first reconstruction was performed at a heart phase of 70 % of the R-peak-to-R-peak interval to select the most suitable images without motion artifacts. Additional reconstructions in 5 % of the steps were performed if motion artifacts were present. Straight multiplanar reconstructions, maximum-intensity projections, and volume-rendering applications of an offline workstation (Ziostation; Amin, Tokyo, Japan) were used to evaluate coronary artery stenosis. At this point, patients with significant coronary artery stenoses with a lumen reduction of 50 % or more were excluded from the study, as this factor might influence the ECG voltage or ST segment.

Second, we measured the LV end-diastolic volume (EDV), end-systolic volume (ESV), ejection fraction, and mass using commercially available, previously validated software [7, 15] (Syngo Circulation 2; Siemens Medical Solutions), and indexed these parameters to the body surface area. For LV volume analyses, serial axial images (slice thickness: 2.0 mm) were reconstructed from the raw data for every 10 % (0–90 %) of the R–R interval. A field of view of 200 × 200 mm^2, 512 × 512 matrix, and medium smooth convolution kernel (B25f) were applied.

Third, LA volume analysis was performed offline using the same software. The maximum LA volume, obtained at end-systole from the phase immediately preceding mitral valve opening, was measured using Simpson's methods, as previously described [8]. The confluence of the pulmonary veins and LA appendage were excluded from the measurements.

Finally, we measured the thickness of the chest wall and the distance from the LV apex to the chest surface, according to the method described in previous reports [12, 13]. In brief, the smallest line from the LV apex to the inner chest wall was identified visually from the axial images obtained in the early systolic phase. Then the sagittal image in which the plane passes through this line was used to measure the distances from the LV apex to the inner chest wall and to the chest surface. The chest-wall thickness was calculated as the difference between the distances from the LV apex to the chest surface and to the inner chest wall. To evaluate the interobserver and intraobserver variability, the determination of the distances from the LV apex to the inner chest wall and to the chest surface of 15 randomly selected patients were performed by two independent observers, and repeated by each observer a week later. Both observers were cardiologists with 3 years of experience in cardiac imaging, who were blinded to the other's findings and the clinical data. The measurement of the distance from the LV apex to the inner chest wall had an intraobserver variability of 12.1 ± 5.8 % with a correlation of 0.99, and an interobserver variability of 12.9 ± 7.8 % with a correlation of 0.99. The measurement of the distance from the LV apex to the chest surface had an intraobserver variability of 4.1 ± 2.3 % with a correlation of 0.98, and an interobserver variability of 6.9 ± 2.7 % with a correlation of 0.94.

Statistical analysis

The results are presented as mean ± standard deviation (SD). The two groups were compared using an unpaired Student's *t* test or a Mann–Whitney *U* test when the variance was heterogeneous. Categorical variables were compared using the Chi-square test. The relations between variables were assessed using Pearson's correlation coefficient. Furthermore, the statistical comparison of parallelism in linear regression was performed using analysis of covariance. Using the LV mass measured by MSCT as a gold standard, the sensitivities, specificities, and positive and negative predictive values of the Sokolow–Lyon voltage criteria and strain pattern as indicators for anatomic LVH were calculated according to standard methods. Multivariate logistic regression analysis was performed to identify independent factors associated with anatomic LVH. Univariate predictors with a P value of less than 0.1 were entered into the multivariate model. The odds ratio and its 95 % confidence interval (CI) for significant independent variables in the multivariate analysis were calculated. All P values were two-sided, and $P < 0.05$ was considered statistically significant.

Results

Clinical and CT findings of the anatomic and nonanatomic LVH groups

The clinical characteristics of the 93 patients are shown in Table 1. Of 93 patients, 23 (25 %) had anatomic LVH and 70 (75 %) did not. There were no statistically significant differences in age, male gender, presence of risk factors, BMI, frequency of patients whose BMI was more than 25 kg/m^2, distance from the heart to the chest surface, and frequency of LVH determined by the Sokolow–Lyon voltage criteria between the anatomic and nonanatomic LVH groups. However, in the anatomic LVH group the systolic blood pressure, LV EDV (index) and ESV (index), LA volume, chest wall thickness, $S_{V1} + R_{V5\ or\ V6}$, frequency of the strain pattern, LVH determined by the

Table 1 Demographic, computed tomographic, and electrocardiographic characteristics according to anatomic left ventricular hypertrophy

	Anatomic LVH ($n = 23$)	Nonanatomic LVH ($n = 70$)	P
Age, years	62 ± 9	62 ± 12	0.793
Male, n	12 (52 %)	47 (67 %)	0.219
Hypertension, n	19 (83 %)	51 (73 %)	0.415
Hypercholesterolemia, n	9 (39 %)	29 (41 %)	0.999
Diabetes mellitus, n	3 (13 %)	12 (17 %)	0.755
Smoking, n	9 (39 %)	22 (31 %)	0.611
Body mass index, kg/m^2	24.6 ± 3.7	23.1 ± 3.8	0.057
Overweight ≥25 kg/m^2, n	8 (35 %)	19 (27 %)	0.597
Blood pressure,, mmHg			
Systolic	147 ± 24	134 ± 27	0.021
Diastolic	83 ± 16	77 ± 13	0.113
EDV, ml	172 ± 79	127 ± 30	0.002
EDV index, ml/m^2	101 ± 40	78 ± 16	0.003
ESV, ml	89 ± 57	48 ± 16	0.005
ESV index, ml/m^2	53 ± 33	29 ± 9	0.004
Ejection fraction, %	51 ± 18	63 ± 9	0.007
LV mass, g	250 ± 81	139 ± 29	0.0001
LV mass index, g/m^2	147 ± 34	85 ± 14	0.0001
Left atrial volume, ml	106 ± 43	73 ± 25	0.001
Distance from heart to the chest surface, cm	3.14 ± 0.95	3.07 ± 0.75	0.883
Chest-wall thickness, cm	2.55 ± 0.91	2.07 ± 0.59	0.014
$S_{V1} + R_{V5}$, mV	3.93 ± 1.32	2.98 ± 1.02	0.002
$S_{V1} + R_{V6}$, mV	3.55 ± 1.38	2.39 ± 0.82	0.0001
LVH by Sokolow–Lyon voltage criteria, %	13 (57 %)	23 (33 %)	0.052
Strain pattern, %	15 (63 %)	9 (13 %)	0.0001
LVH by Sokolow–Lyon voltage criteria with strain pattern, %	11 (48 %)	8 (11 %)	0.0005
LVH by Sokolow–Lyon voltage criteria without strain pattern, %	2 (9 %)	15 (21 %)	0.224
Strain pattern without LVH by Sokolow–Lyon voltage criteria, %	4 (17 %)	1 (1 %)	0.013

Values represent mean ± standard deviation (SD) or n (percentage). Anatomic LVH was diagnosed if the LV mass index was >104 g/m^2 in women or >116 g/m^2 in men

LVH left ventricular hypertrophy, *EDV* end-diastolic volume, *ESV* end-systolic volume, *LV* left ventricular

Sokolow–Lyon voltage criteria with the strain pattern, and the strain pattern without LVH determined by the Sokolow–Lyon voltage criteria were significantly larger, and the ejection fraction significantly smaller, than in the nonanatomic LVH group.

Performance of the Sokolow–Lyon voltage criteria and strain pattern in the detection of anatomic LVH

Table 2 shows the sensitivity, specificity, and predictive values of the Sokolow–Lyon voltage criteria, strain pattern, and both as indicators of anatomic LVH. The Sokolow–Lyon voltage criteria had a sensitivity of 57 %, specificity of 67 %, positive predictive value of 36 %, and negative predictive value of 82 %. By contrast, the strain pattern had a sensitivity of 65 %, specificity of 87 %, positive predictive value of 63 %, and negative predictive value of 88 %. The Sokolow–Lyon voltage criteria with the strain pattern had a sensitivity of 48 %, specificity of 89 %, positive predictive value of 58 %, and negative predictive value of 84 %.

As shown in Fig. 2, $S_{V1} + R_{V5}$ showed a positive correlation with the LV mass index (all patients: $r = 0.522$, $P < 0.0001$; overweight: $r = 0.618$, $P < 0.001$; nonoverweight: $r = 0.482$, $P < 0.0001$). The slope did not significantly differ between the two groups.

Multivariate logistic regression analysis

To identify the independent factors associated with anatomic LVH, multivariate logistic regression analysis was performed using BMI, systolic blood pressure, EDV index, ejection fraction, LA volume, chest wall thickness, LVH by Sokolow–Lyon voltage criteria, and the strain pattern (using variables with P values <0.1 on univariate analysis). Multivariate analysis revealed that the ejection fraction and strain pattern remained associated with the presence of anatomic LVH (Table 3). However, the Sokolow–Lyon voltage was not associated with anatomic LVH.

Discussion

The present study demonstrates the relationship between the Sokolow–Lyon ECG voltage criteria or strain pattern

Table 2 Performance of the Sokolow–Lyon electrocardiographic voltage criteria and strain pattern for the detection of anatomic left ventricular hypertrophy

	Sokolow–Lyon voltage	Strain pattern	Sokolow–Lyon voltage with strain pattern
Sensitivity	57	65	48
Specificity	67	87	89
PPV	36	63	58
NPV	82	88	84

Values represent percentages

PPV positive predictive value, *NPV* negative predictive value

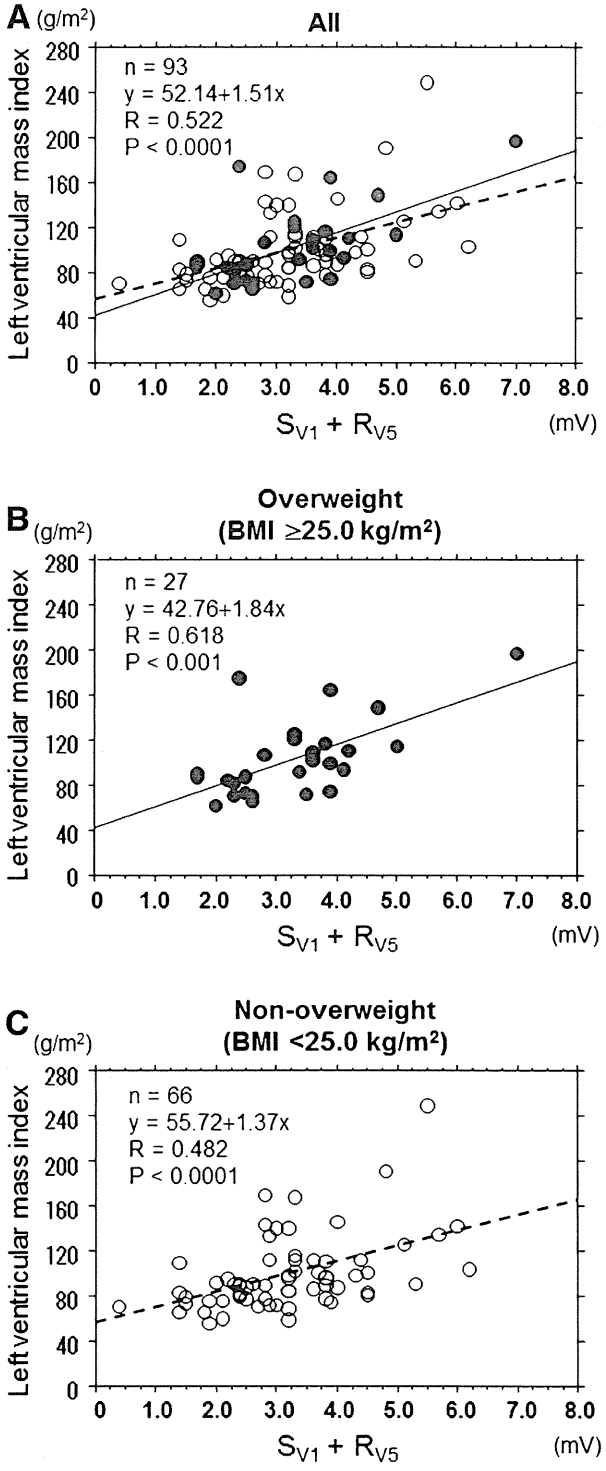

Fig. 2 Correlations between $S_{V1} + R_{V5}$ and the left ventricular mass index in all patients (**a**), overweight patients (**b**), and nonoverweight patients (**c**). *BMI* body mass index

and several important factors, including LV volume and mass, LA volume, chest-wall thickness, and the distance from the heart to the chest surface. Multivariate analysis

Table 3 Multivariate logistic regression analysis

	Odds ratio	95 % CI	*P*
Body mass index	0.997	0.759–1.308	0.981
Systolic blood pressure	1.031	0.993–1.071	0.106
EDV index	1.015	0.970–1.061	0.523
Ejection fraction	0.916	0.851–0.986	0.020
Left atrial volume	1.020	0.997–1.044	0.095
Chest-wall thickness	3.318	0.700–15.734	0.131
LVH by Sokolow–Lyon voltage criteria	0.338	0.043–2.640	0.301
Strain pattern	23.460	2.811–195.777	0.004

CI confidence interval, *EDV* end-diastolic volume, *LVH* left ventricular hypertrophy

revealed that the strain pattern was more closely associated with anatomic LVH than was the Sokolow–Lyon voltage.

Several studies have reported that the ECG amplitude is influenced by the patient's body size. Abergel et al. [16] demonstrated that the sensitivity of the standard Sokolow–Lyon voltage criteria was much lower in obese patients than in nonobese patients. Moreover, Horton et al. [17] reported that the distance from the heart to the chest surface influences the amplitude of the recorded precordial voltage. They calculated the distance from the chest surface to the mid-LV using echocardiography. However, they did not consider the chest-wall thickness and LA size. The Sokolow–Lyon voltage is the sum of two precordial voltages, which are both dependent on the distance between the heart and the electrode (chest surface). In our previous study [13], the Sokolow–Lyon voltage showed a stronger association with the distance to the chest surface, which correlated with body-size measurements such as BMI. Therefore, the sensitivity and negative predictive value of the Sokolow–Lyon voltage in the obese patients were lower than those in the nonobese patients. By contrast, the specificity and positive predictive value of the Sokolow–Lyon voltage in the obese patients were higher than those in the nonobese patients. In the present study, $S_{V1} + R_{V5}$ showed a positive correlation with the LV mass index, although the slope did not significantly differ between the overweight and nonoverweight groups. The prevalence of obesity in the patient population studied may have influenced these results. Therefore, in the clinical setting the body size should be taken into account when interpreting Sokolow–Lyon voltage results.

By contrast, the strain pattern was independently associated with the presence of anatomic LVH. Okin et al. [4] demonstrated that the strain pattern is associated with increased LV mass and a high prevalence of anatomic LVH, and that the combination of the strain pattern and

increased LV mass on echocardiography markedly increases the risk of cardiovascular disease and all-cause mortality [5]. Thus far, several previous studies examining the prognostic effects of LVH have used two-dimensional echocardiography with direct visualization of the myocardium and real-time imaging [4, 5]. Two-dimensional echocardiography can detect LVH by measuring the LV wall thickness. However, this modality is operator dependent, and may be impaired by a poor acoustic window and inadequate endocardial border discrimination in 5–10 % of patients [18]. Moreover, assumption of the geometric shape for both M-mode and two-dimensional echocardiography may lead to errors, particularly because variations in ventricular geometry affect the calculated LV mass. It is likely that three-dimensional echocardiography will become the technique of choice for precise LV mass measurements. On the other hand, three-dimensional MSCT used in the present study shows excellent definition of the endocardial and epicardial borders [7, 15]. Using MSCT as a gold standard for LVH assessment, Truong et al. [19] reported the diagnostic performance of seven ECG-based LVH criteria. Their data revealed that the ECG criteria for LVH have high specificities, with the Cornell-based criteria providing the best test performance for identifying patients with LVH. We also reported the overall superiority of Cornell voltage over Sokolow–Lyon voltage for the detection of LVH [13]. As the Cornell voltage is the sum of the precordial and limb voltages, this result would be less dependent on chest-wall thickness. However, Truong et al. also did not consider the effect of chest-wall thickness. MSCT allowed us to evaluate not only the LV mass, LA volume, and coronary arteries more precisely than echocardiography, but also the distance from the heart to the chest surface or the chest-wall thickness from the same scan, regardless of body size. It should be noted that no patient was excluded from cardiac quantitative assessment with MSCT because of poor image quality.

Finally, the history of traditional risk factors, such as hypertension and diabetes mellitus, were not associated with anatomic LVH in the present study. Hence the comprehensive factors, such as severity, duration, or control status of disease, would lead to concentric LVH, which may have a more important impact than the history of risk factors. Further studies are needed to clarify these complex relationships.

Study limitations

There are several limitations in the present study. First, LV mass calculations were performed using software on ECG-gated cardiac MSCT scans alone. Magnetic resonance (MR) imaging is considered the gold standard for the assessment of LV function and mass. However, the availability of cardiac MR scanners capable of cardiac imaging and the skilled personnel needed to obtain and interpret the imaging results limits widespread clinical application of this technique. Furthermore, cardiac MR image acquisition is relatively time consuming. By contrast, MSCT has advantages over cardiac MR imaging in terms of image-acquisition time and its widespread availability, despite the relatively high radiation dose and requirement of iodinated contrast material. Therefore, it is important to obtain as much relevant information using the same data set as acquired for noninvasive coronary angiography, although we could not adopt MSCT as the primary method of determining LV mass. Second, the population was highly selective; patients with atrial fibrillation, bundle branch block, or significant coronary artery stenosis, and a history of myocardial infarction, previous coronary artery bypass grafting, or percutaneous transluminal intervention were excluded. Thus, our findings may not apply to more general populations. Third, ECG measurements were obtained from a single tracing, although measurement variability on ECG has been reported. Finally, the number of patients examined was very small. Multivariate analysis revealed that the odds ratio of the strain pattern was relatively high, but the 95 % CI was wide. This may have limited the precision and statistical power of the study.

Conclusions

This MSCT study demonstrated that even after removing the effects of various factors, the strain pattern was still associated with the presence of anatomic LVH, whereas the Sokolow–Lyon voltage was not. In the clinical setting, this finding should be taken into account in the interpretation of LVH detected using 12-lead ECG.

Conflict of interest The authors declare that there are no financial or other relationships that could lead to a conflict of interest.

References

1. Levy D, Salomon M, D'Agostino RB, Belanger AJ, Kannel WB (1994) Prognostic implications of baseline electrocardiographic features and their serial changes in subjects with left ventricular hypertrophy. Circulation 90:1786–1793
2. Okin PM, Devereux RB, Nieminen MS, Jern S, Oikarinen L, Viitasalo M, Toivonen L, Kjeldsen SE, Julius S, Dahlöf B (2001) Relationship of the electrocardiographic strain pattern to left ventricular structure and function in hypertensive patients: the LIFE study. Losartan Intervention For End point. J Am Coll Cardiol 38:514–520
3. Casale PN, Devereux RB, Alonso DR, Campo E, Kligfield P (1987) Improved sex-specific criteria of left ventricular hypertrophy for clinical and computer interpretation of electrocardiograms: validation with autopsy findings. Circulation 75:565–572

4. Okin PM, Devereux RB, Fabsitz RR, Lee ET, Galloway JM, Howard BV, Strong Heart Study (2002) Quantitative assessment of electrocardiographic strain predicts increased left ventricular mass: the Strong Heart Study. J Am Coll Cardiol 40:1395–1400
5. Okin PM, Roman MJ, Lee ET, Galloway JM, Howard BV, Devereux RB (2004) Combined echocardiographic left ventricular hypertrophy and electrocardiographic ST depression improve prediction of mortality in American Indians: the Strong Heart Study. Hypertension 43:769–774
6. Molloy TJ, Okin PM, Devereux RB, Kligfield P (1992) Electrocardiographic detection of left ventricular hypertrophy by the simple QRS voltage-duration product. J Am Coll Cardiol 20:1180–1186
7. Okuyama T, Ehara S, Shirai N, Sugioka K, Ogawa K, Oe H, Kitamura H, Itoh T, Otani K, Matsuoka T, Inoue Y, Ueda M, Hozumi T, Yoshiyama M (2008) Usefulness of three-dimensional automated quantification of left ventricular mass, volume, and function by 64-slice computed tomography. J Cardiol 52:276–284
8. Takagi Y, Ehara S, Okuyama T, Shirai N, Yamashita H, Sugioka K, Kitamura H, Ujino K, Hozumi T, Yoshiyama M (2009) Comparison of determinations of left atrial volume by the biplane area-lengthy and Simpson's methods using 64-slice computed tomography. J Cardiol 53:257–264
9. Ehara S, Shirai N, Okuyama T, Matsumoto K, Matsumura Y, Yoshiyama M (2011) Absence of left ventricular concentric hypertrophy: a prerequisite for zero coronary calcium score. Heart Vessels 26:487–494
10. Ehara S, Matsumoto K, Shirai N, Nakanishi K, Otsuka K, Iguchi T, Hasegawa T, Nakata S, Yoshikawa J, Yoshiyama M (2013) Typical coronary appearance of dilated cardiomyopathy versus left ventricular concentric hypertrophy: coronary volumes measured by multislice computed tomography. Heart Vessels 28: 188–198
11. Suenari K, Nakano Y, Hirai Y, Ogi H, Oda N, Makita Y, Ueda S, Kajihara K, Tokuyama T, Motoda C, Fujiwara M, Chayama K, Kihara Y (2013) Left atrial thickness under the catheter ablation lines in patients with paroxysmal atrial fibrillation: insights from 64-slice multidetector computed tomography. Heart Vessels 28:360–368
12. Ehara S, Okuyama T, Shirai N, Oe H, Matsumura Y, Sugioka K, Itoh T, Otani K, Hozumi T, Yoshiyama M, Yoshikawa J (2010) Comprehensive evaluation of the apex beat using 64-slice computed tomography: impact of left ventricular mass and distance to chest wall. J Cardiol 55:256–265
13. Ehara S, Shirai N, Matsumoto K, Okuyama T, Matsumura Y, Yoshikawa J, Yoshiyama M (2011) The clinical value of apex beat and electrocardiography for the detection of left ventricular hypertrophy from the standpoint of the distance factors from the heart to the chest wall: a multislice CT study. Hypertens Res 34:1004–1010
14. Okin PM, Oikarinen L, Viitasalo M, Toivonen L, Kjeldsen SE, Nieminen MS, Edelman JM, Dahlöf B, Devereux RB, LIFE Study Investigators (2011) Serial assessment of the electrocardiographic strain pattern for prediction of new-onset heart failure during antihypertensive treatment: the LIFE study. Eur J Heart Fail 13:384–391
15. Mühlenbruch G, Das M, Hohl C, Wildberger JE, Rinck D, Flohr TG, Koos R, Knackstedt C, Günther RW, Mahnken AH (2006) Global left ventricular function in cardiac CT. Evaluation of an automated 3D region-growing segmentation algorithm. Eur Radiol 16:1117–1123
16. Abergel E, Tase M, Menard J, Chatellier G (1996) Influence of obesity on the diagnostic value of electrocardiographic criteria for detecting left ventricular hypertrophy. Am J Cardiol 77: 739–744
17. Horton JD, Sherber HS, Lakatta EG (1977) Distance correction for precordial electrocardiographic voltage in estimating left ventricular mass: an echocardiographic study. Circulation 55:509–512
18. Malm S, Frigstad S, Sagberg E, Larsson H, Skjaerpe T (2004) Accurate and reproducible measurement of left ventricular volume and ejection fraction by contrast echocardiography: a comparison with magnetic resonance imaging. J Am Coll Cardiol 44:1030–1035
19. Truong QA, Ptaszek LM, Charipar EM, Taylor C, Fontes JD, Kriegel M, Irlbeck T, Toepker M, Schlett CL, Bamberg F, Blankstein R, Brady TJ, Nagurney JT, Hoffmann U (2010) Performance of electrocardiographic criteria for left ventricular hypertrophy as compared with cardiac computed tomography: from the Rule Out Myocardial Infarction Using Computer Assisted Tomography trial. J Hypertens 28:1959–1967

European Heart Journal – Cardiovascular Imaging (2014) **15**, 332–340
doi:10.1093/ehjci/jet232

Prognosis of vulnerable plaque on computed tomographic coronary angiography with normal myocardial perfusion image

Kenichiro Otsuka[1], Shota Fukuda[2]*, Atsushi Tanaka[3], Koki Nakanishi[1], Haruyuki Taguchi[2], Minoru Yoshiyama[1], Kenei Shimada[1], and Junichi Yoshikawa[4]

[1]Department of Internal Medicine and Cardiology, Osaka City University Graduate School of Medicine, Osaka, Japan; [2]Department of Medicine, Osaka Ekisaikai Hospital, 2-1-10 Honden, Nishi-Ku, Osaka 550-0022, Japan; [3]Department of Cardiovascular Medicine, Social Insurance Kinan Hospital, Tanabe, Japan; and [4]Nishinomiya Watanabe Cardiovascular Center, Nishinomiya, Japan

Received 8 August 2013; revised 6 October 2013; accepted after revision 11 October 2013; online publish-ahead-of-print 7 November 2013

Aims Increasing clinical evidence has emphasized the importance of coronary plaque characteristics, rather than the severity of luminal narrowing on acute coronary syndrome (ACS) outcome. Computed tomographic coronary angiography (CTCA) is a unique, non-invasive approach for assessing plaque characteristics. This study was prospectively designed to investigate the prognostic value of physiologically non-obstructive but a vulnerable coronary plaque on CTCA for predicting future ACS events.

Methods and results This study consisted of 543 patients who had undergone CTCA and had normal findings on exercise-stress myocardial perfusion single-photon emission computed tomography. CTCA analysis included the presence of >50% luminal stenosis and vulnerable features including positive remodelling (PR), low-attenuation plaque, and ring-like sign. The primary endpoint was ACS events including cardiac death, non-fatal myocardial infarction, and unstable angina. The mean follow-up period was 3.4 ± 0.8 years. The 3-year cumulative event rate was 1.2% per year, and 87% of ACS events occurred in plaques with at least one of vulnerable features. In patient-based multivariate analysis, the presence of plaque with vulnerable features on CTCA was a significant predictor for future ACS events ($P = 0.001$). Patients with vulnerable plaque had worse ACS outcomes compared with those without vulnerable plaques (3-year cumulative event rate; 3.2 per year vs. 0.8%, $P < 0.001$).

Conclusion This study demonstrated that physiologically non-obstructive but vulnerable coronary plaques were associated with future ACS events. We should pay more attention to currently non-obstructive plaque but showing vulnerable morphologies on CTCA.

Keywords acute coronary syndrome • computed tomographic angiography • prognosis

Introduction

Myocardial perfusion on exercise-stress single-photon emission computed tomography (SPECT) is an established gold standard technique for physiological assessment of luminal narrowing. Because normal findings on myocardial perfusion SPECT are associated with benign outcomes,[1–4] a plaque showing a normal myocardial perfusion image has been disregarded in terms of predicting future acute coronary syndrome (ACS) events.

Computed tomographic coronary angiography (CTCA) has emerged as an accurate and non-invasive imaging modality that can identify plaque composition as well as the severity of coronary artery lumen narrowing.[5–8] Recent CTCA studies have shown that certain plaque morphologies on CTCA, including positive remodelling (PR), low-attenuation plaque (LAP), and ring-like sign, are closely associated with future ACS events.[9,10] A recent intravascular ultrasound study suggested the importance of assessing plaque characteristics for predicting ACS events, irrespective of coronary artery luminal narrowing.[11] However,

* Corresponding author. Tel: +81 6 6581 2881; Fax: +81 6 6584 1807, Email: h-syouta@mve.biglobe.ne.jp

discussion still remains whether plaques that do not cause physiological obstruction but have vulnerable characteristics have any clinical significance for predicting future ACS events. This prospective study aimed to investigate the prognostic importance of CTCA-featured plaque characteristics on the occurrence of future ACS events in patients with normal findings on exercise-stress myocardial perfusion SPECT.

Methods

Study population

During the period from April 2007 to March 2011, consecutive 1956 patients who prospectively underwent CTCA for chest pain ($n = 1212$) or multiple coronary artery disease (CAD) risk factors ($n = 744$) were screened for participation in the present study. Patients gave written informed consent before the CTCA examinations, and patients with coronary plaques on CTCA who had normal SPECT results were followed. The exclusion criteria were (i) previous history of coronary artery bypass grafting, (ii) previous history of myocardial infarction, and (iii) valvular heart disease of more than moderate severity. Based on the findings of CTCA, patients with normal coronary arteries (no plaque) ($n = 390$) and patients who required coronary angiography and/or revascularization ($n = 406$) were excluded. Also, patients were excluded when at least one major coronary artery segment was uninterpretable to analyse due to motion artefacts or heavy calcification ($n = 19$). Following the protocol, 762 patients were referred for exercise stress SPECT within 4 weeks after CTCA examination (19 ± 8 days), and 567 patients showed normal myocardial perfusion SPECT. Patients lost to follow-up were excluded at the time of the last follow-up assessment ($n = 24$). The final study population consisted of 543 patients (344 men, mean age 65 ± 10 years). An exclusion flow diagram was summarized in *Figure 1*. Blood samples were taken at the CTCA examination to measure serum creatinine, fasting lipids, glucose, glycated haemoglobin, and C-reactive protein (CRP). All patients received optimized medical therapy for atherosclerotic risk factors according to the American College of Cardiology Foundation/American Heart Association (ACCF/AHA) guidelines based on structured interviews by the attending physicians. Each patient was followed once every 2 months until the end of the study or the occurrence of ACS events using structured interviews and clinical examinations by physicians. This study design was approved by the Institutional Review Board of Osaka Ekisaikai Hospital.

Scan protocol and image reconstruction

The CTCA was performed using a SOMATOM Sensation 64 system (Siemens Medical Systems, Forchheim, Germany), with the following scan parameters: 64 × 0.6 mm collimation, tube voltage of 120 kV, gantry rotation time of 330 ms, and tube current of 770–850 mA. For the contrast-enhanced scans, 50–80 mL of non-ionic contrast agent (Omnipaque 350, Daiichi Sankyo Co, Tokyo, Japan) was injected intravenously at a flow rate of 3.5–5.5 mL/s followed by 30 mL of saline. Delay time was defined using the bolus tracking technique with a region of interest positioned at the level of the ascending aorta in the monitoring scan and using a manually triggered threshold of 100 Hounsfield units (HU) for the main scanning. All patients received 5 mg of bisoprolol orally before the computed tomography (CTCA) scan, and patients with a heart rate >70 beats/min received 2 mg of metoprolol intravenously. In addition, patients received 0.6 mg of sublingual nitroglycerin. All scans were performed during a single breath hold. The raw data were reconstructed using algorithms optimized for electrocardiography-gated multi-slice spiral reconstruction. Retrospective gating was used and the estimated radiation dose was 9 mSv.

Analysis of CTCA

All three major vessels were assessed in every patient using the modified 17-segment AHA model for coronary segment classification. In each coronary artery segment, coronary atherosclerotic plaque was defined as a tissue structure >1 mm^2 that existed either within the coronary artery lumen or adjacent to the coronary artery lumen and that could be discriminated from the surrounding pericardial tissue, epicardial fat, or the vessel lumen itself.[10,12] The severity of luminal-diameter stenosis was visually divided into (i) <50% luminal stenosis, (ii) 50–69% luminal stenosis, or (iii) >70% luminal stenosis. The vessel was displayed on axial images and multi-planar reconstruction images, and diameter stenosis was estimated using proximal and distal reference segments. The reference segment was the most adjacent points to the maximal stenosis at which there was minimal or no plaque. Each plaque was classified as follows: (i) non-calcified plaque = plaque with lower density compared with the contrast-enhanced vessel lumen without any calcification (>150 HU), (ii) calcified plaque = plaque with predominantly calcification, or (iii) mixed plaque = plaque with a small amount of calcification elements within a single plaque.[10]

In non-calcified and mixed plaques, the presence or absence of the following three vulnerable features was analysed: LAP, PR, and ring-like sign. First, non-calcified plaques were divided into LAP (plaques with <30 HU) and intermediate-attenuation plaques (plaques between 30 and 150 HU).[9,10] To identify the presence of LAP, a region of interest was placed on at least five randomly selected points within each plaque, and the mean value was defined as the plaque density. Secondly, the remodelling index was defined as the ratio of the vessel diameter at the plaque site to the reference diameter set proximal to the lesion in a normal-appearing vessel segment. The presence of PR was defined as a remodelling index >1.1.[9,10] Finally, a ring-like sign represented a plaque core with low attenuation surrounded by a rim-like area of higher attenuation. The ring-like sign was defined by the following criteria: (i) the presence of a ring of high attenuation around certain coronary artery plaques and (ii) CTCA attenuation of the ring, presenting higher than those of the adjacent plaque and no >150 HU.[10,13] *Figure 2* shows a representative case of vulnerable featured plaque on CTCA that resulted in an ACS event.

All CTCA data sets were analysed on a per-segment basis by two independent experienced readers (A.T. and K.S.) who had >5-year experience in CTCA analysis with the number of CTCA examinations compatible with ACCF/AHA clinical competence statement training level 3.[14] In case of disagreement or intermediate CTCA results, the plaques were reevaluated for the consensus judgement. They were blinded to clinical characteristics and the results of SPECT until the end of patient's enrolment period in this study (March 2011).

Myocardial perfusion image acquisition and analysis

Each patient underwent ECG-gated myocardial perfusion SPECT with symptom-limited exercise on a bicycle. The endpoints included excessive fatigue, dyspnoea, moderate-to-severe angina, hypotension, diagnostic ST depression, or significant arrhythmia. At peak exercise, thallium-201 (^{201}TL) was injected intravenously, and the patient was encouraged to exercise for another 1 min. Initial images were obtained immediately after the termination of exercise and delayed images were obtained 4 h later. Patients were asked to refrain from ingesting caffeine-containing beverages for at least 12 h, nitrates and calcium channel blockers for 24 h, and β-blockers for 48 h, before the myocardial perfusion study. Gated SPECT studies were performed with a 2-head gamma camera (GCA-7200; Toshiba Medical Systems, Otawara, Japan) equipped with low-energy, general-purpose collimators, with the detectors set to form a 180° angle. Sixty equidistant projections were acquired over

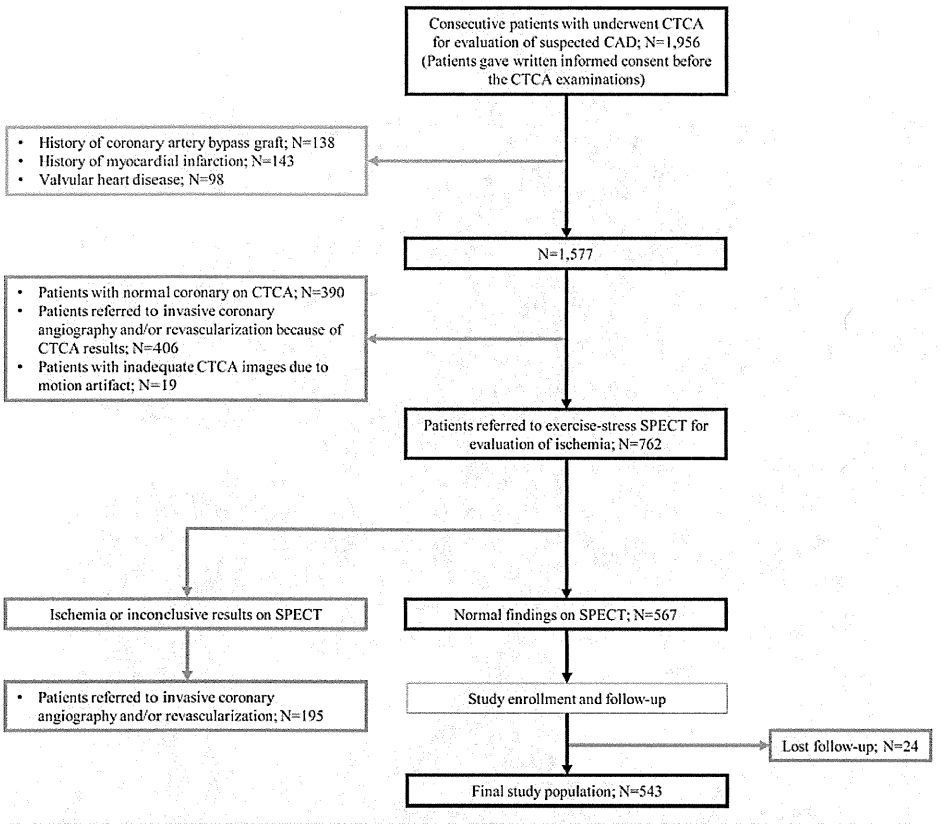

Figure 1 Flow diagram of patient enrolment. CTCA, computed tomographic coronary angiography; SPECT, single-photon emission computed tomography.

360° in a 64 × 64 matrix. Acquisition of images was performed with 30 s per step, in 6° angular steps. For all patients, SPECT image set was reconstructed at a dedicated workstation (GCA-7200; Toshiba Medical Systems, Otawara, Japan) into short-axis, vertical long-axis, and horizontal long-axis sections encompassing the entire left ventricle. No attenuation correction was applied. In addition, polar maps of perfusion were produced using a dedicated software package (GCA-7200; Toshiba Medical Systems, Otawara, Japan).

Myocardial perfusion SPECT image interpretation was visually performed by two experienced cardiologists (H.T. and S.F.) with 10 years of experience in cardiac radionuclide imaging who were blinded to CTCA findings. If the discordance between two experienced cardiologists did not resolve, SPECT finding was defined as 'inconclusive results'. Also, patients who did not reach to the target heart rate, defined as [220 − age (years) × 0.85], were classified into 'inconclusive results'. Normal myocardial perfusion SPECT was defined as myocardial perfusion without any perfusion abnormalities. Further, increased lung up take of ^{201}TL, transient left ventricular dilatation at initial image, and decreased myocardial ^{201}TL washout were defined as abnormal myocardial perfusion that suggest multi-vessel CAD.[4,15,16] When there was discordance between them, a consensus reading was obtained.

Endpoints

The pre-specified endpoint of this study was the occurrence of an ACS event defined as cardiac death, non-fatal myocardial infarction, and unstable angina requiring revascularization. Myocardial infarction was defined by the ACCF/AHA guideline, and unstable angina was defined according to the Braunwald classification. The culprit lesion was comprehensively determined on the basis of the association of invasive coronary angiography with electrocardiographic changes, echocardiography, or myocardial ischaemia as detected during a stress test. When culprit lesion was difficult to determine by imaging modalities, stress test was performed after medical therapy to stabilize the patient's condition. Unstable angina requiring revascularizations was included in endpoints. All events of unstable angina were proved by invasive coronary angiography.

Statistical analysis

Categorical variables are presented as number (%) and continuous variables as mean ± SD. The χ^2 test was used for comparison of categorical variables. Between-group comparisons were made using the independent-samples *t*-test or Mann–Whitney *U* test as appropriate. Multivariate Cox proportional hazard analysis was performed to identify predictors of ACS events on per-patient based analysis, including hypertension, 50–69% luminal stenosis, 2- or 3-vessel disease, and vulnerable featured plaques. The Kaplan–Meier survival method was used to compare survival according to the existence or absence of vulnerable features on CTCA for per-segment and per-patient-based analyses, using the log-rank test. A P value < 0.05 was considered statistically significant.

The sample size was calculated to provide adequate statistical power for identifying plaque characteristics that result in ACS events on the basis of a range of assumptions about the frequency of vulnerable plaques: power of 80%, hazard ratio of 5.0, ACS event rate for vulnerable

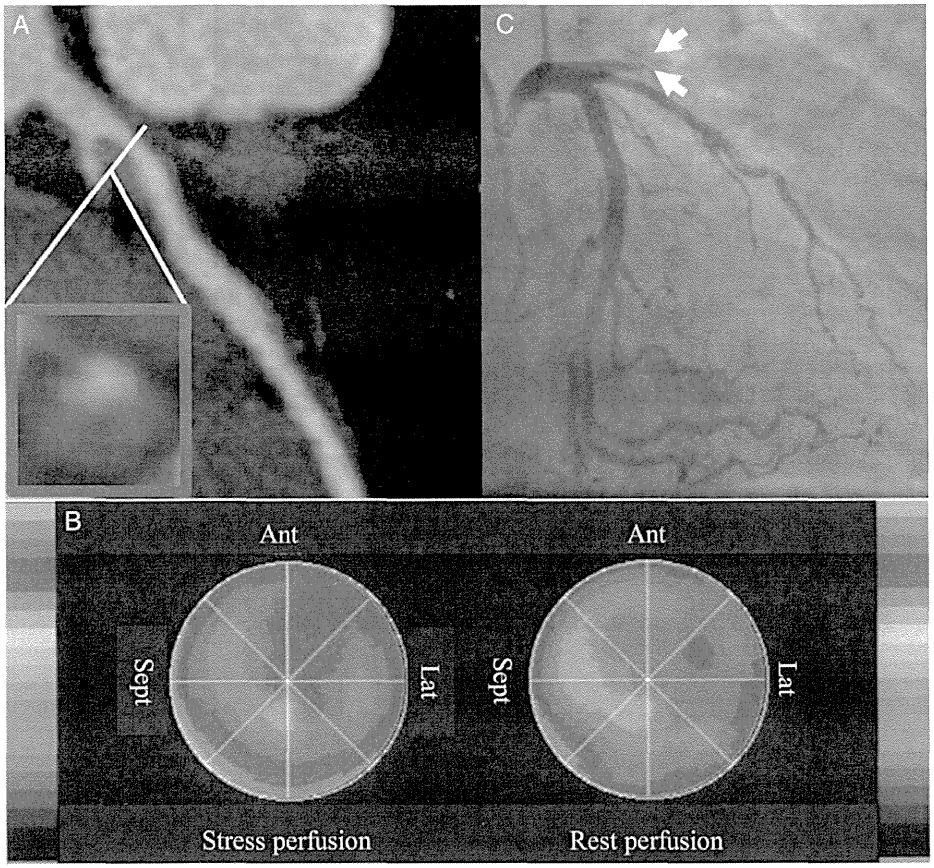

Figure 2 A representative case of CTCA with a vulnerable featured plaque and normal perfusion imaging on SPECT and subsequent ACS events. (*A*) CTCA image shows an atherosclerotic plaque with high-risk signs of PR, low-attenuation, and ring-like sign at the proximal LAD. (*B*) Stress-rest SPECT perfusion polar maps show normal perfusion. (*C*) One-year later, acute myocardial infarction occurred at the high-risk plaque. Invasive coronary angiography showed the total occlusion of LAD artery (arrows). ACS, acute coronary syndrome; CTCA, computed tomographic coronary angiography; LAD, left anterior descending artery; SPECT, single-photon emission computed tomography.

featured plaques of 5%, and a two-sided alpha of 0.050. If a vulnerable featured plaque is detected in 30% of patients with CAD, 518 patients would be needed. Allowing for a 5% attrition rate, we calculated that we would need to enrol 545 patients.

Results

Baseline plaque compositions on CTCA

Of the 543 patients, 9231 segments were adequately analysed where 1107 plaques were detected (2.0 plaques per patient). The severity of luminal narrowing was <50% in 774 (70%) plaques and between 50 and 70% in 331 (30%) plaques. No plaques had luminal narrowing with >70%. At least one of the vulnerable features, including PR, LAP, or ring-like sign, was detected in 274 plaques (24%) in 182 patients (33%; 0.4 plaques per patient). PR was detected in 183 (16%) plaques, LAP in 133 (12%), and ring-like sign in 30 (2.7%). Of these, 44 plaques (3.9%) had any 2 vulnerable features, and 14 plaques (1.2%) had all 3 vulnerable features, respectively. These results are summarized in *Figure 3*. The plaques with any vulnerable features were 85 (31%) in the right coronary artery, 25 (9.1%) in the left main coronary artery, 118 (43%) in the left anterior descending coronary artery, and 45 (16%) in the left circumflex coronary artery.

Patients' characteristics and ACS events

Patients were divided into two groups: with or without plaques with at least one of vulnerable features on CTCA (*Table 1*). Patients with at least one of vulnerable features had lower HDL-cholesterol levels than those with no vulnerable features (49 ± 14 vs. 56 ± 18 mg/dL, $P = 0.014$). There were no significant differences in other clinical characteristics, the medications that the patients were taking after CTCA and myocardial perfusion SPECT, and laboratory examinations between patients with and without vulnerable features. Also, clinical characteristics, plaque features and drugs of patients with ACS event, lost at the follow-up, and positive SPECT results are shown in Supplementary data online, *Table S1*.

Of the 543 patients, the composite ACS event was examined after a mean follow-up of 3.4 ± 0.8 years (range 1–5.4 years; median 3.4

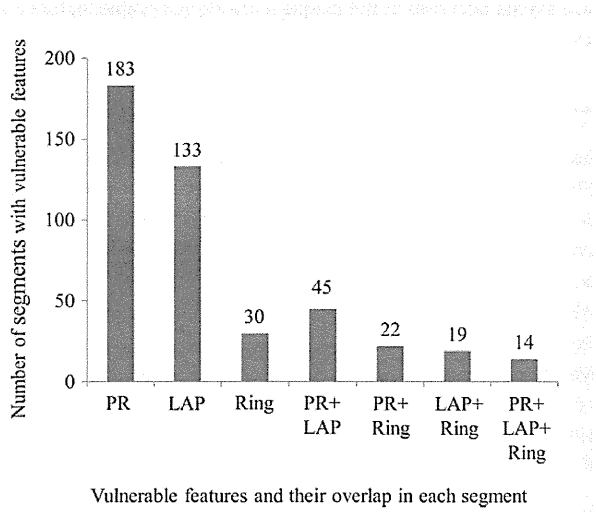

Figure 3 Overlapping of three CTCA features. LAP, low-attenuation plaque; PR, positive remodelling.

years). During this period, 23 ACS events occurred (1.2% per year), comprising myocardial infarction in 12 patients and unstable angina requiring revascularizations in 11 patients. Three of 12 patients with myocardial infarction died during the hospitalization thereafter. All culprit lesions were confirmed by emergent invasive coronary angiography. Of the 23 ACS events, the number of vulnerable features on CTCA in the culprit lesion was 3 in 5 (22%) patients, 2 in 8 (35%) patients, 1 in 7 (30%) patients, and 0 in 3 (13%) patients. Of the 182 patients with plaques with vulnerable features, 20 patients developed ACS events. Remaining 162 patients had no event. On the other hand, only three patients suffered ACS events in patients without plaques with vulnerable features.

Predictors for future ACS events

Supplementary data online, *Table S2* shows the patient-based univariate analysis compared between patients with and without ACS event. Patients with ACS event had higher prevalence of hypertension ($P = 0.046$), 50–69% luminal stenosis ($P < 0.001$), 2- or 3-vessel disease ($P < 0.001$), and vulnerable featured plaques ($P < 0.001$) than those without ACS event. In patient-based multivariate analysis, the presence of plaque with vulnerable features on CTCA was a significant predictor for future ACS events ($P = 0.001$) (*Table 2*). *Figure 4* shows the Kaplan–Meier curve of patients according to the presence of plaques with vulnerable features (*Figure 4A*), the extent of atherosclerotic burden (*Figure 4B*), and the severity of luminal stenosis (*Figure 4C*), respectively. Kaplan–Meier analysis confirmed that patients with vulnerable featured plaques on CTCA had a worse outcome compared with those without vulnerable featured plaques ($P < 0.001$) in *Figure 4A*. The event rate in patients with and without vulnerable featured plaques was 3.2 and 0.24% per year, respectively.

The results of segment-based univariate and multivariate analyses are provided in Supplementary data online, *Tables S3 and S4*. The segment-based Kaplan–Meier analysis according to the presence or absence of the three CTCA features for future ACS events is shown in *Figure 5*. The presence of any of the three vulnerable features on CTCA correlated with ACS, with a graded relationship with the number of vulnerable features (*Figure 5*). The results of sensitivity, specificity, positive predictive value (PPV), and negative predictive value (NPV) of vulnerable plaques for predicting ACS events are summarized in *Table 3*. The presence of >1 vulnerable feature showed a high PPV of 87%, and the absence of two or three vulnerable features showed a high NPV of 97% for predictive value of developing future ACS event.

Table 1 Patient characteristics of those with or without vulnerable featured plaques

	Patients with vulnerable plaques ($n = 182$)	Patients without vulnerable plaques ($n = 361$)	*P* value
Clinical characteristics			
Male gender, *n* (%)	123 (67)	221 (61)	0.14
Age, years	66 ± 10	65 ± 11	0.08
Hypertension, *n* (%)	118 (65)	224 (62)	0.52
Dyslipidaemia, *n* (%)	105 (57)	184 (51)	0.15
Diabetes, *n* (%)	91 (50)	149 (41)	0.053
Current smoking, *n* (%)	44 (29)	64 (28)	0.73
Body mass index, kg/m^2	24.5 ± 3.6	24.1 ± 3.7	0.35
Laboratory data			
Total cholesterol, mg/dL	195 ± 42	195 ± 40	0.98
Triglycerides, mg/dL	148 ± 89	149 ± 97	0.81
LDL cholesterol, mg/dL	128 ± 37	121 ± 36	0.11
HDL cholesterol, mg/dL	49 ± 14	54 ± 18	0.014
Fasting glucose, mg/dL	122 ± 30	122 ± 43	0.97
HbA1c, %	6.2 ± 1.3	6.0 ± 1.0	0.084
CRP, mg/L	1.6 ± 1.9	1.3 ± 2.1	0.21
Medications after CTCA and myocardial perfusion SPECT			
Aspirin, *n* (%)	159 (87)	279 (81)	0.10
Beta blocker, *n* (%)	39 (22)	88 (28)	0.12
ACE inhibitor or ARB, *n* (%)	111 (62)	219 (67)	0.19
Calcium blocker, *n* (%)	58 (32)	124 (39)	0.13
Statin, *n* (%)	134 (74)	267 (74)	0.81

Values are mean ± SD or *n* (percentage). The column showed *P* values for the comparison between patients with and without vulnerable featured plaques. ACE, angiotensin converting enzyme; ACS, acute coronary syndrome; ARB, angiotensin receptor blocker; CRP, C-reactive protein; CTCA, computed tomographic coronary angiography; HDL, high-density lipoprotein; LDL, low-density lipoprotein; SPECT, single-photon emission computed tomography.

Discussion

This CTCA study revealed that ACS events occurred at the rate of 1.2% per year in patients with normal myocardial perfusion image. Patients having a vulnerable plaque on CTCA showed poorer prognoses compared with those without vulnerable plaque, and most

Table 2 Patient-based multivariate predictors of ACS events during follow-up

	Hazard ratio (95% CI)	*P* value
Hypertension	1.7 (0.55–5.36)	0.34
50–69% luminal stenosis	1.9 (0.54–6.94)	0.30
2- or 3-vessel disease	2.2 (0.75–6.66)	0.14
Vulnerable featured plaques	9.4 (2.66–33.4)	0.001

The variables entered into patient-based multivariate Cox proportional hazards model when they indicated $P < 0.05$ in *Table 2*. Less than 50% luminal stenosis was excluded because it was initially associated with 50–69% luminal stenosis. The final variables entered were hypertension, 50–69% luminal stenosis, 2- or 3-vessel disease, and vulnerable featured plaques. ACS, acute coronary syndrome; CI, confidence interval.

ACS events occurred at the plaque showing vulnerable features on baseline CTCA.

CTCA predictors for ACS events

Assessment of coronary artery stenosis and plaque characteristics by CTCA has been well validated in prior studies against intracoronary ultrasonography/virtual histology and optical coherence tomography.[7,8,17] Early CTCA reports indicated that the presence and extent of obstructive CAD defined by coronary plaques causing >50% reduction in the luminal diameter is a valuable prognostic marker of incident death or major adverse cardiovascular events.[18,19] Recent CTCA studies identified plaque compositions, including PR, LAP, and ring-like sign as vulnerable features associated with plaques that are prone to rupture, independent of the severity of coronary artery luminal stenosis.[9,10,20] These findings were

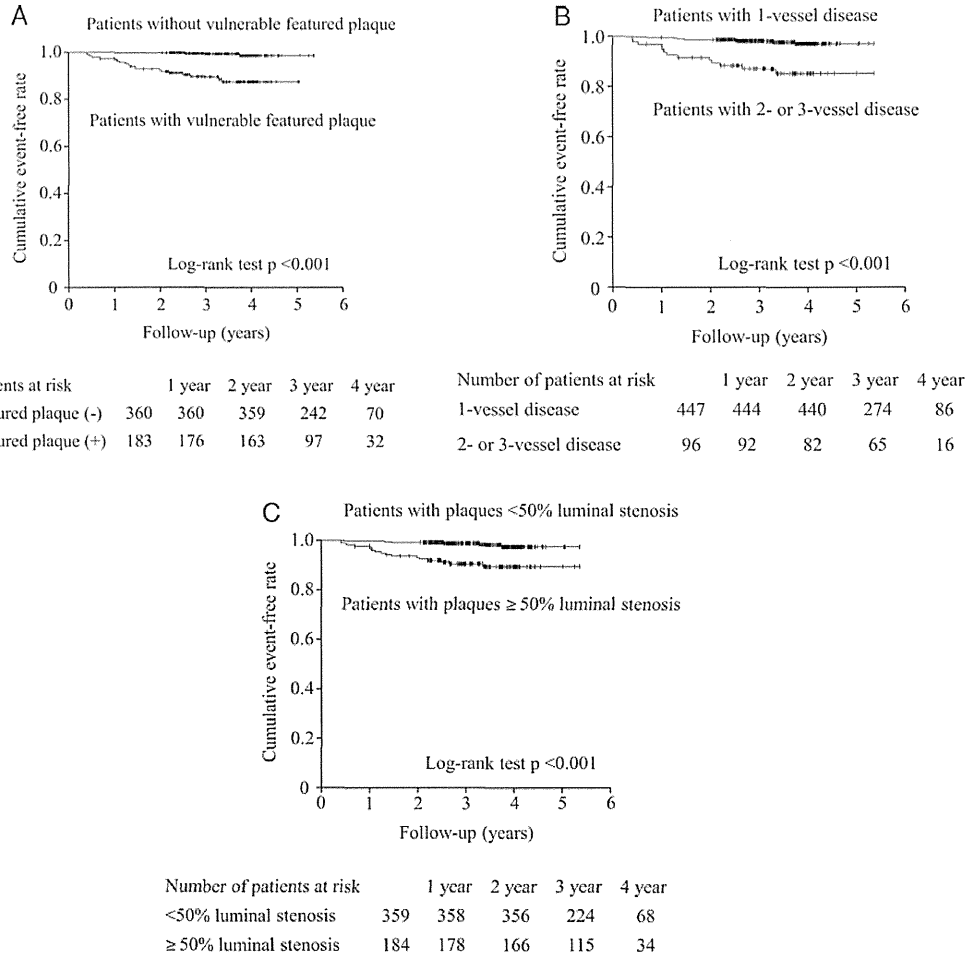

Figure 4 Kaplan–Meier analyses for future ACS events. (*A*) The Kaplan–Meier curve according to the presence of plaques with vulnerable features (no vulnerable features, 1 vulnerable feature, and >2 vulnerable features). (*B*) The Kaplan–Meier curve in the comparison between patients with 1-vessel disease vs. patients with two- to three-vessel disease. (*C*) The Kaplan–Meier curve of patients with plaques >50% (50–69%) luminal stenosis vs. patients with plaques <50% luminal stenosis. ACS, acute coronary syndrome.

supported by the investigation with intravascular ultrasound demonstrated that coronary lesions responsible for cardiac events were associated with the large plaque burden, a small lumen area, and thin-cap fibroatheroma morphology.[11] It should be emphasized, however, that almost all of these studies investigated plaque extent and stenosis severity, and there are only limited data on the relationship between atherosclerotic plaque morphology and regional myocardial ischaemia attributed to the atherosclerotic lesion in patients with CAD.[21,22] Specifically, the use of CTCA has methodological limitations with regard to the use of diameter stenosis for assessing coronary artery stenosis severity.[8] This was the first study that used SPECT to confirm that most coronary atherosclerotic lesions associated with future ACS events were physiologically non-obstruction.

In this study, 29% of plaques ($n = 331$) with luminal narrowing between 50 and 70% showed normal perfusion patterns. This finding was similar to previous observations. Schuijf *et al.*[23] underwent both CTCA and myocardial perfusion imaging on SPECT in 114 patients. They found ~50% of patients with plaques with >50% luminal narrowing on CTCA who showed a normal findings on SPECT. Van Werkhoven *et al.*[21] demonstrated that 75 of 158 patients (48%) with plaques with >50% luminal narrowing on CTCA had normal SPECT results.

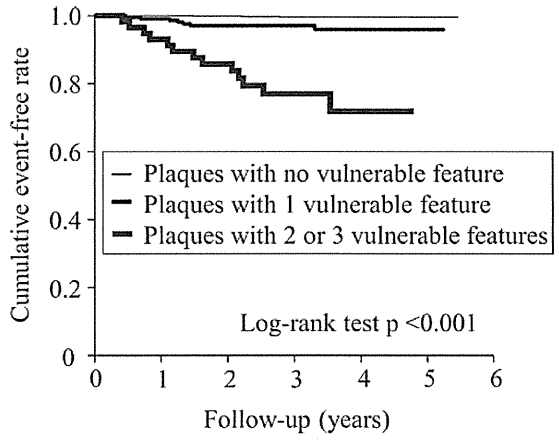

Figure 5 Segment-based Kaplan–Meier analyses for future ACS events. Segment-based Kaplan–Meier curve according to the presence or absence of the three CTCA features for future ACS events (plaques with no vulnerable feature, one vulnerable feature, and two or three vulnerable features).

On the other hand, previous CTCA studies showed that the absence of plaque conveys a benign prognosis for symptomatic patients being evaluated for CAD.[18,19] The low event rate for those with normal CTCA findings is comparable to the event rate among healthy low-risk individuals (<1%).[18] This study showed that physiologically non-obstructive and no vulnerable plaques observed on CTCA warrant an excellent prognosis, even in the presence of atherosclerotic plaques (0.55%; 0.16% per year), indicating the importance of assessing plaque composition for risk stratification of patients with CAD.

ACS outcome in comparison with previous studies

The rate of ACS events in the present study (1.2% per year) seems to be slightly higher than that reported in previous studies among patients with normal myocardial perfusion SPECT varied from 0 to 0.93% per year,[2,4,5] in which unstable angina was not included as the primary endpoint, at least partially due to the subjective judgement of unstable angina. The optimal management is required in patients with unstable angina to prevent serious adverse outcomes.[24] The endpoint of this study included only unstable angina requiring revascularization.

In recent investigations using CTCA and intravascular ultrasound, the event rate of recurrent coronary events (except revascularizations for stent restenosis) among ACS patients ranged from 2.2–5.5% per year,[11,25,26] which was comparable to that of patients with vulnerable featured plaques in the present study (3.2% per year). Data from large-scale clinical trials that used statins for secondary prevention in patients with previous myocardial infarction showed a similar event rate (2.0–2.9% per year).[27,28] These findings could justify the assessment of vulnerable plaques without abnormalities using myocardial perfusion for predicting future ACS events. If CTCA would detect plaques showing vulnerability, more aggressive intervention and/or close monitoring might be required even with normal finding on myocardial perfusion SPECT.

Study limitations

There are several limitations in this study. First, regional wall motion and the left ventricular ejection fraction, which may have incremental diagnostic value in patients with multi-vessel CAD, were not assessed

Table 3 Diagnostic accuracy of CTCA characteristics for prediction of ACS events during follow-up

CCTA characteristics	Sensitivity (%)	Specificity (%)	PPV (%)	NPV (%)	Accuracy (%)
PR	8.7	99	69	84	11
LAP	7.1	98	56	84	6.5
Ring-like sign	30	98	39	98	23
Any one of vulnerable features	7.3	99	86	76	20
Two or three vulnerable features	28	99	56	97	30

ACS, acute coronary syndrome; CTCA, computed tomographic coronary angiography; LAP, low-attenuation plaque; NPV, negative predictive value; PPV, positive predictive value; PR, positive remodelling.

in SPECT analysis. Quantitative analysis should be performed in the future studies. In this study, however, none of the patients had severe coronary stenosis of >70% or multi-vessel CAD. Therefore, these technical limitations might not affect the results of the present study. Secondly, we observed three ACS events (unstable angina) from the calcified plaques during the 3-year follow-up. Despite calcified nodules being recognized as a type of causing coronary thrombosis not caused by plaque rupture or erosion,[29] inconsistent results have been observed for the association between calcified nodules and future ACS events.[19] Three vulnerable features were evaluated in non-calcified and mixed plaques in the present study. Vulnerable features were not assessed in plaques with predominant calcification (calcified plaque), because plaques carrying heavy calcification are difficult to assess by CTCA. Therefore, the impact of vulnerable features in plaques with calcification on ACS outcome remained unclear. Further investigation is required to elucidate the relationship between the amount and characteristics of calcification and its impact in the prediction of future ACS events. Thirdly, all of the 24 patients that were lost in the follow-up had no vulnerable featured plaques on CTCA. However, patients with normal CTCA (no plaques) and those with abnormal SPECT results were not followed, and their prognostic data were unknown. Fourthly, the severity of CAD risk factors and concomitant medications for diabetes were not taken into account for the analysis, although these factors may influence on the outcome in patients with CAD. Finally, radiation exposure may preclude the widespread use of CTCA in clinical practice. Recent CTCA algorithms, including prospective gating methods and tube current modulation, may overcome this limitation.[30]

Conclusions

This CTCA study revealed that vulnerable plaques on CTCA, even those that were normal on myocardial perfusion image, were associated with future ACS events. We should pay more attention to plaques showing normal myocardial perfusion image but vulnerability.

Supplementary data

Supplementary data are available at *European Heart Journal – Cardiovascular Imaging* online.

Acknowledgements

We appreciate the assistance of following colleagues in the recording and management of CTCA data sets and patient records: Makoto Sakamoto MT, Keisuke Iwata MT, and Chihiro Kakoiyama, RN (Osaka Ekisaikai Hospital).

Conflict of interest: The authors declare no conflict of interest.

References

1. Hachamovitch R, Berman DS, Shaw LJ, Kiat H, Cohen I, Cabico JA *et al.* Incremental prognostic value of myocardial perfusion single photon emission computed tomography for the prediction of cardiac death : differential stratification for risk of cardiac death and myocardial infarction. *Circulation* 1998;**97**:535–43.
2. Metz LD, Beattie M, Hom R, Redberg RF, Grady D, Fleischmann KE. The prognostic value of normal exercise myocardial perfusion imaging and exercise echocardiography: a meta-analysis. *J Am Coll Cardiol* 2007;**49**:227–37.
3. Matsuo S, Nakajima K, Horie M, Nakae I, Nishimura T. Prognostic value of normal stress myocardial perfusion imaging in Japanese population. *Circ J* 2008;**72**:611–7.
4. Bourque JM, Beller GA. Stress myocardial perfusion imaging for assessing prognosis: an update. *JACC Cardiovasc Imaging* 2011;**4**:1305–19.
5. Schroeder S, Kopp AF, Baumbach A, Meisner C, Kuettner A, Georg C *et al.* Noninvasive detection and evaluation of atherosclerotic coronary plaques with multislice computed tomography. *J Am Coll Cardiol* 2001;**37**:1430–5.
6. Achenbach S, Moselewski F, Ropers D, Ferencik M, Hoffmann U, MacNeill B *et al.* Detection of calcified and noncalcified coronary atherosclerotic plaque by contrast-enhanced, submillimeter multidetector spiral computed tomography: a segment-based comparison with intravascular ultrasound. *Circulation* 2004;**109**:14–7.
7. Motoyama S, Kondo T, Sarai M, Sugiura A, Harigaya H, Sato T *et al.* Multislice computed tomographic characteristics of coronary lesions in acute coronary syndromes. *J Am Coll Cardiol* 2007;**50**:319–26.
8. Voros S, Rinehart S, Qian Z, Joshi P, Vazquez G, Fischer C *et al.* Coronary atherosclerosis imaging by coronary CT angiography: current status, correlation with intravascular interrogation and meta-analysis. *JACC Cardiovasc Imaging* 2011;**4**:537–48.
9. Motoyama S, Sarai M, Harigaya H, Anno H, Inoue K, Hara T *et al.* Computed tomographic angiography characteristics of atherosclerotic plaques subsequently resulting in acute coronary syndrome. *J Am Coll Cardiol* 2009;**54**:49–57.
10. Otsuka K, Fukuda S, Tanaka A, Nakanishi K, Taguchi H, Yoshikawa J *et al.* Napkin-ring sign on coronary CT angiography for the prediction of acute coronary syndrome. *JACC Cardiovasc Imaging* 2013;**6**:448–57.
11. Stone GW, Maehara A, Lansky AJ, de Bruyne B, Cristea E, Mintz GS *et al.* A prospective natural-history study of coronary atherosclerosis. *N Engl J Med* 2011;**364**:226–35.
12. Leber AW, Knez A, Becker A, Becker C, Ziegler FV, Nikolaou K *et al.* Accuracy of multidetector spiral computed tomography in identifying and differentiating the composition of coronary atherosclerotic plaques A comparative study With intracoronary ultrasound. *J Am Coll Cardiol* 2004;**43**:1241–7.
13. Kashiwagi M, Tanaka A, Kitabata H, Tsujioka H, Kataiwa H, Komukai K *et al.* Feasibility of noninvasive assessment of thin-cap fibroatheroma by multidetector computed tomography. *JACC Cardiovasc Imaging* 2009;**2**:1412–9.
14. Budoff MJ, Cohen MC, Garcia MJ, Hodgson JM, Hundley WG, Lima JA *et al.* ACCF/AHA clinical competence statement on cardiac imaging with computed tomography and magnetic resonance. *Circulation* 2005;**112**:598–617.
15. Kaminek M, Myslivecek M, Skvarilova M, Husak V, Koranda P, Metelkova I *et al.* Increased prognostic value of combined myocardial perfusion SPECT imaging and the quantification of lung Tl-201 uptake. *Clin Nucl Med* 2002;**27**:255–60.
16. Abidov A, Bax JJ, Hayes SW, Hachamovitch R, Cohen I, Gerlach J *et al.* Transient ischemic dilation ratio of the left ventricle is a significant predictor of future cardiac events in patients with otherwise normal myocardial perfusion SPECT. *J Am Coll Cardiol* 2003;**42**:1818–25.
17. Ito T, Terashima M, Kaneda H, Nasu K, Matsuo H, Ehara M *et al.* Comparison of in vivo assessment of vulnerable plaque by 64-slice multislice computed tomography versus optical coherence tomography. *Am J Cardiol* 2011;**107**:1270–7.
18. Hulten EA, Carbonaro S, Petrillo SP, Mitchell JD, Villines TC. Prognostic value of cardiac computed tomography angiography: a systematic review and meta-analysis. J Am Coll Cardiol 2011;**57**:1237–47.
19. Bamberg F, Sommer WH, Hoffmann V, Achenbach S, Nikolaou K, Conen D *et al.* Meta-analysis and systematic review of the long-term predictive value of assessment of coronary atherosclerosis by contrast-enhanced coronary computed tomography angiography. *J Am Coll Cardiol* 2011;**57**:2426–36.
20. Nakanishi K, Fukuda S, Shimada K, Ehara S, Inanami H, Matsumoto K *et al.* Non-obstructive low attenuation coronary plaque predicts three-year acute coronary syndrome events in patients with hypertension: multidetector computed tomographic study. *J Cardiol* 2012;**59**:167–75.
21. van Werkhoven JM, Schuijf JD, Gaemperli O, Jukema JW, Boersma E, Wijns W *et al.* Prognostic value of multislice computed tomography and gated single-photon emission computed tomography in patients with suspected coronary artery disease. *J Am Coll Cardiol* 2009;**53**:623–32.
22. Motoyama S, Sarai M, Inoue K, Kawai H, Ito H, Harigaya H *et al.* Morphologic and functional assessment of coronary artery disease. *Circ J* 2013;**77**:411–7.
23. Schuijf JD, Wijns W, Jukema JW, Atsma DE, de Roos A, Lamb HJ *et al.* Relationship between noninvasive coronary angiography with multi-slice computed tomography and myocardial perfusion imaging. *J Am Coll Cardiol* 2006;**48**:2508–14.
24. Anderson JL, Adams CD, Antman EM, Bridges CR, Califf RM, Casey DE Jr *et al.* 2011 ACCF/AHA focused update incorporated into the ACC/AHA 2007 guidelines for the management of patients With unstable angina/Non-ST-elevation myocardial infarction: a report of the American College of Cardiology Foundation/American Heart Association TASK Force on Practice Guidelines. *Circulation* 2011;**123**:e426–579.
25. Kristensen TS, Kofoed KF, Kuhl JT, Nielsen WB, Nielsen MB, Kelbaek H. Prognostic implications of nonobstructive coronary plaques in patients with non-ST-segment elevation myocardial infarction: a multidetector computed tomography study. *J Am Coll Cardiol* 2011;**58**:502–9.
26. Miyauchi K, Daida H, Morimoto T, Hiro T, Kimura T, Nakagawa Y *et al.* Reverse vessel remodeling but not coronary plaque regression could predict future cardiovascular

events in ACS patients with intensive statin therapy—the extended JAPAN-ACS study. *Circ J* 2012;**76**:825–32.
27. Pedersen TR, Faergeman O, Kastelein JJ, Olsson AG, Tikkanen MJ, Holme I *et al.* High-dose atorvastatin vs usual-dose simvastatin for secondary prevention after myocardial infarction: the IDEAL study: a randomized controlled trial. *JAMA* 2005; **294**:2437–45.
28. Armitage J, Bowman L, Wallendszus K, Bulbulia R, Rahimi K, Haynes R *et al.* Intensive lowering of LDL cholesterol with 80 mg versus 20 mg simvastatin daily in 12,064 survivors of myocardial infarction: a double-blind randomised trial. *Lancet* 2010; **376**:1658–69.
29. Virmani R, Kolodgie FD, Burke AP, Farb A, Schwartz SM. Lessons from sudden coronary death: a comprehensive morphological classification scheme for atherosclerotic lesions. *Arterioscler Thromb Vasc Biol* 2000;**20**:1262–75.
30. Halliburton SS, Abbara S, Chen MY, Gentry R, Mahesh M, Raff GL *et al.* SCCT Guidelines on radiation dose and dose-optimization strategies in cardiovascular CT. *J Cardiovasc Comput Tomogr* 2011;**5**:198–224.

27. Groenwold RHH, Donders ART, Roes KCB, Harrell FE, Moons KGM. Dealing with missing outcome data in randomized trials and observational studies. *Am J Epidemiol* 2012;**175**:210–7.
28. Van Buuren S, Groothuis-oudshoorn K. Journal of Statistical Software MICE: multivariate imputation by chained. *J Stat Softw* 2011;**45**:1–67.
29. Cheitlin MD, Armstrong WF, Aurigemma GP, Beller GA, Bierman FZ, Davis JL *et al.* ACC/AHA/ASE 2003 guideline update for the clinical application of echocardiography. *Circulation* 2003;**108**:1146–62.
30. Zamorano JL, Badano LP, Bruce C, Chan KL, Gonçalves A, Hahn RT *et al.* EAE/ASE recommendations for the use of echocardiography in new transcatheter interventions for valvular heart disease. *J Am Soc Echocardiogr* 2011;**24**:937–65.
31. Dávila-Román VG, Phillips KJ, Daily BB, Dávila RM, Kouchoukos NT, Barzilai B. Intraoperative transoesophageal echocardiography and epiaortic ultrasound for assessment of atherosclerosis of the thoracic aorta. *J Am Coll Cardiol* 1996;**28**:942–7.
32. Ledley RS, Lusted LB. Reasoning foundations of medical diagnosis. *Science* 1959;**130**: 9–21.
33. Moons KGM, Van Es GA, Deckers JW, Habbema JDF, Grobbee DE. Limitations of sensitivity, specificity, likelihood ratio, and Bayes' theorem in assessing diagnostic probabilities. *Epidemiology* 1997;**8**:12–7.
34. Miettinen OS, Henschke CI, Yankelevitz DF. Evaluation of diagnostic imaging tests. *J Clin Epimiol* 1998;**51**:1293–8.
35. Moons KGM. Criteria for scientific evaluation of novel markers: a perspective. *Clin Chem* 2010;**56**:537–41.
36. Bossuyt PMM, Reitsma JBR, Linnet K, Moons KGM. Beyond diagnostic accuracy: the clinical utility of diagnostic tests. *Clin Chem* 2012;**58**:1636–43.
37. Ferrante di Ruffano L, Hyde CJ, McCaffery KJ, Bossuyt PMM, Deeks JJ. Assessing the value of diagnostic tests: a framework for designing and evaluating trials. *Br Med J* 2012;**344**:e686.
38. Kurra V, Lieber ML, Sola S, Kalahasti V, Hammer D, Gimple S *et al.* Extent of thoracic aortic atheroma burden and long-term mortality after cardiothoracic surgery: a computed tomography study. *J Am Coll Cardiol* 2010;**3**:1020–9.
39. Lee R, Matsutani N, Polimenakos AC, Levers LC, Lee M, Johnson RG. Preoperative noncontrast chest computed tomography identifies potential aortic emboli. *Ann Thorac Surg* 2007;**84**:38–41.
40. Barazangi N, Wintermark M, Lease K, Rao R, Smith W, Josephson SA. Comparison of computed tomography angiography and transesophageal echocardiography for evaluating aortic arch disease. *Stroke* 2011;**20**:436–42.
41. Kim SS, Hijazi ZM, Lang RM, Knight BP. The use of intracardiac echocardiography and other intracardiac imaging tools to guide noncoronary cardiac interventions. *J Am Coll Cardiol* 2009;**53**:2117–28.
42. Bartel T, Müller L, Müller S. Intra-aortic phased-array imaging: new guiding tool for transcatheter aortic valve implantation. *Eur Heart J* 2009;**30**:2368.

IMAGE FOCUS

doi:10.1093/ehjci/jet262
Online publish-ahead-of-print 26 December 2013

Giant mycotic coronary aneurysm associated with late stent infection

Shinichi Nonin[1], Takao Hasegawa[1]*, Hidekazu Hirai[2], Shigefumi Suehiro[2], and Minoru Yoshiyama[1]

[1]Department of Cardiovascular Medicine, Graduate School of Medicine, Osaka City University, 1-4-3 Asahi-machi, Abeno-ku, Osaka 545-8585, Japan and [2]Department of Cardiovascular Surgery, Graduate School of Medicine, Osaka City University, Osaka, Japan

* Corresponding author. Tel: +81 66645 3801; Fax: +81 66646 6808, E-mail: takao0321@aol.com

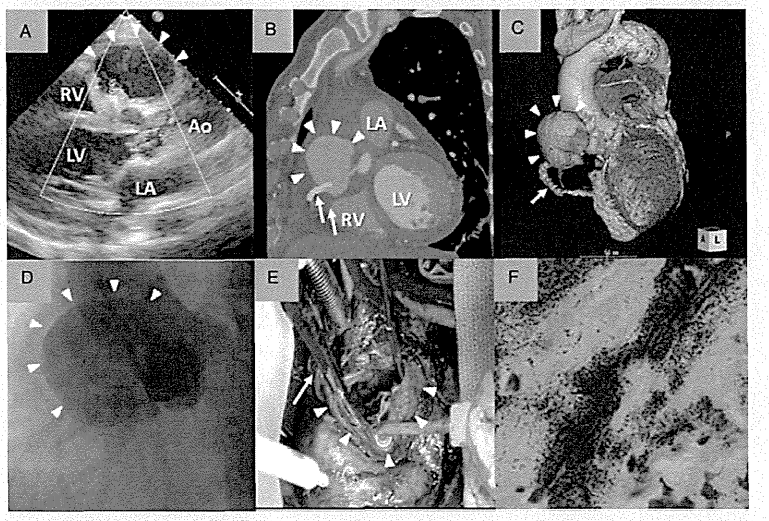

A 67-year-old man with a history of paclitaxel-eluting stent implantation in the right coronary artery (RCA) 4 years previously needs below-the-knee amputation of the right leg due to uncontrollable foot infection. The patient had acute high fever and leukocytosis, and performed repeatedly transthoracic echocardiography (TTE) to rule out infective endocarditis. TTE revealed the presence of a mass (4.7 × 3.4 cm) (head arrows) adjacent to the sinus of Valsalva (*Panel A*). A giant pseudoaneurysm (5.1 × 3.7 cm) (head arrows) at the proximal site of the stent (arrows) was confirmed by the cardiovascular computed tomography (CCT; *Panel B*) and also a three-dimensional volume rendered CCT image (*Panel C*). The angiography in the left anterior oblique projection showed contrast agent extravasation into a giant mycotic pseudoaneurysm (arrows) (*Panel D*). We performed emergent surgery to decrease the risk for acute rupture since the mycotic pseudoaneurysm progressed rapidly in 2 weeks. An intraoperative image showed the pseudoaneurysm after opening and aspiration of the cavity (head arrows), and the stent removed from the RCA (arrow) (*Panel E*). Haematoxylin–eosin stain (×250) showed only fibrous tissue without normal arterial walls and the presence of inflammation with accumulation of neutrophils and cocci (*Panel F*).

Coronary stent infection is a rare complication, but it is associated with high mortality. Late stent infection may be caused by drug-eluting stent (DES)-related local problems (delayed endothelialization of the stent struts, inhibition of neointimal growth, late acquired incomplete stent apposition, and coronary aneurysm formation). These local reactions to the DES may provide a nidus for stent infection during an episode of bacteraemia.

European Heart Journal – Cardiovascular Imaging (2014) **15**, 284–291
doi:10.1093/ehjci/jet158

Insulin resistance is associated with coronary plaque vulnerability: insight from optical coherence tomography analysis

Tomokazu Iguchi*, Takao Hasegawa, Kenichiro Otsuka, Kenji Matsumoto, Takanori Yamazaki, Satoshi Nishimura, Shinji Nakata, Shoichi Ehara, Toru Kataoka, Kenei Shimada, and Minoru Yoshiyama

Department of Cardiovascular Medicine, Osaka City University, Asahi-machi, Abeno-ku, Osaka 545-8585, Japan

Received 15 May 2013; accepted after revision 4 August 2013; online publish-ahead-of-print 9 September 2013

Aims Previous studies have reported that insulin resistance plays an important role in the progression of atherosclerosis. However, the relationship between insulin resistance and coronary plaque instability is not well established. The purpose of this study was to assess the relationship between insulin resistance and coronary plaque characteristics identified by optical coherence tomography (OCT).

Methods and results This study enrolled 155 consecutive patients undergoing percutaneous coronary intervention. OCT image acquisitions were performed in the culprit lesions. Insulin resistance was identified using the homeostasis model assessment of insulin resistance (HOMA-IR). Subjects were divided into three tertiles according to the HOMA-IR values. Patients in the higher HOMA tertile had more frequent prevalence of lipid-rich plaques than those in the middle and lower tertiles (83 vs. 62 vs. 57%; $P = 0.01$). The thin-cap fibroatheroma (TCFA) prevalence rates among the higher (>2.5), middle (1.4–2.5), and lower HOMA-IR (<1.4) tertiles were 50, 29, and 26% ($P = 0.02$). The microvessel prevalence rates of the three tertiles were 54, 39, and 28% ($P = 0.02$). Furthermore, in the higher HOMA-IR group, the fibrous cap was significantly thinner compared with the other two tertiles (vs. lower HOMA-IR, $P = 0.009$; vs. middle HOMA-IR, $P = 0.008$). On multivariate analysis, acute coronary syndrome [odds ratio (OR): 17.98; 95% confidence interval (CI): 7.12−52.02; $P < 0.0001$] and HOMA-IR >2.50 (OR: 3.57; 95% CI: 1.42−9.55; $P = 0.007$) were independent predictors for the presence of TCFA.

Conclusion This study suggests that insulin resistance might be associated with coronary plaque vulnerability.

Keywords Insulin resistance • Vulnerable plaque • Optical coherence tomography

Introduction

Diabetes mellitus (DM) is a well-known risk factor for adverse cardiovascular events and an independent poor prognostic predictor in patients with coronary artery disease (CAD).[1–3] Several studies demonstrated that diabetic patients exhibit coronary plaque progression and increased coronary plaque vulnerability.[4–7] In the process of promoting atherogenesis, hyperinsulinaemia resulting from insulin resistance plays an important role. Previous studies have suggested that insulin has direct atherogenic effects such as enhancement of vascular smooth muscle cell proliferation,[8] and several epidemiological studies demonstrated that insulin resistance was associated with an increased risk of CAD in various ethnicities.[9–11] However, few studies have examined the relationship between the degree of insulin resistance and coronary plaque vulnerability. In a previous analysis using conventional intravascular ultrasound (IVUS) and integrated backscatter IVUS (IB-IVUS), insulin resistance and hyperinsulinaemia were significantly associated with an increased lipid-rich plaque content.[12,13] Although IVUS is a widely used invasive imaging technique for evaluating the coronary plaque features, optical coherence tomography (OCT) is a recent newly developed modality with a high resolution (10 μm). OCT can detect coronary

* Corresponding author. Tel: +81 66645 3801; Fax: +81 66646 6808, Email: t.igu74@gmail.com

plaque morphology, including microthrombi, ruptured plaques, and vulnerable plaques represented by thin-cap fibroatheroma (TCFA) more accurately than IVUS.

Homeostasis model assessment of insulin resistance (HOMA-IR) has been commonly used as a surrogate marker of insulin resistance in daily clinical practice because this simple index could evaluate insulin resistance easily and this index correlates quite well with the glucose clamp technique, recognized as the gold standard method for the estimation of insulin resistance.[14] There is no report on the association between insulin resistance and coronary plaque characteristics identified by OCT. In this study, we aimed to examine the relationship between insulin resistance as measured by the HOMA-IR and coronary plaque vulnerability assessed by OCT.

Methods

Study population

From August 2008 to October 2012, 169 consecutive patients with CAD [including acute coronary syndrome (ACS) and stable angina pectoris (SAP)] who underwent percutaneous coronary intervention (PCI) for *de novo* culprit coronary lesions with OCT guidance and with a blood sample for glucometabolic parameter measurement at the Osaka City University were enrolled in the present study. The exclusion criteria included patients with congestive heart failure, cardiogenic shock, serum creatinine level >2 mg/dL, an intercurrent infection or other inflammatory disease, left main coronary artery lesions, total occlusions, fast plasma glucose level >140 mg/dL, patients with insulin therapy, and poor OCT image quality for analysis. Finally, according to these exclusion criteria, we enrolled 155 consecutive patients in this study. This study was approved by the hospital ethics committee, and all subjects provided informed consent before participation.

Definition of clinical diagnosis

In the present study, SAP was defined as no change in frequency, duration, or intensity of chest symptoms in the 4 weeks before intervention. ACS included unstable angina pectoris and myocardial infarction (MI). Unstable angina pectoris was defined as a progressive crescendo pattern or angina at rest without an increase in cardiac enzyme levels. MI was defined as the presence of continuous typical chest symptoms for >30 min, diagnostic electrocardiographic changes of ST-segment elevation or depression, cardiac enzyme levels of more than twice the upper limit of the normal range, and local cardiac wall motion asynergy on echocardiography. DM was identified by a diabetic clinical history or fasting plasma glucose level ≥126 mg/dL, 2 h post-load glucose level ≥200 mg/dL, glycosylated haemoglobin (HbA1c) level ≥6.5%, and/or the use of hypoglycaemic agents. Insulin resistance was estimated by the HOMA-IR values, calculated as [fasting insulin (μU/mL) × fasting plasma glucose (mg/dL)/405]. Various serum markers were measured by commercial radioimmunoassay kits and specific immunoradiometric assays. Blood samples for the assessment of glucometabolic and lipid parameters [total cholesterol, triglyceride, high-density lipoprotein (HDL) cholesterol, and low-density lipoprotein (LDL) cholesterol levels] were collected from the patients after a 12 h overnight fast.

Angiographic analysis

All patients received oral aspirin (100 mg/day) and clopidgrel (300 mg loading dosage, 75 mg/day) or ticlopidine (200 mg/day) before the procedure. A 5-Fr or 6-Fr guiding catheter was used to selectively cannulate the ostium of target coronary artery through the femoral or radial artery. All captured angiographic images were analysed *with* offline quantitative coronary analysis (QAngio XA 7.2; Medis Medical Imaging Systems, Leiden, The Netherlands) by two experienced observers who were unaware of clinical information and results of the OCT analysis. The minimal lumen diameter, distal reference, proximal reference, reference diameter, percentage of diameter stenosis, and lesion length with the least foreshortening view were measured for the culprit lesion using standard techniques.[15] The culprit lesion was determined based on the findings of coronary angiogram, electrocardiogram, transthoracic echocardiography, and/or myocardial perfusion scintigraphy.

OCT image acquisition

After the diagnostic angiography, an additional intravenous heparin at a dose of 100 U/kg was injected for the OCT examination. If the coronary flow was Thrombolysis In Myocardial Infarction grade 0, I, II, aspiration thrombectomy was performed using an aspiration catheter (Thrombuster II, Kaneka Corporation, Japan). After administration of intracoronary nitroglycerin (100–200 μg), OCT was performed before predilation with a balloon catheter for the culprit lesion. Images were acquired using the time-domain (M2 OCT Imaging System, LightLab Imaging, Westford, MA, USA) or frequency-domain (C7 OCT Intravascular Imaging System, St Jude Medical, St Paul, MN, USA) OCT system. The intracoronary OCT imaging technique has been described previously.[16] Briefly, the M2 system uses a 3 F occlusion balloon catheter, and commercially available dextran was infused into the coronary artery from the distal tip of the occlusion balloon catheter at 0.5 mL/s by an injector to remove the blood from the field of view. The 0.016-inch imaging wire was automatically pulled back from a distal to a proximal position at a rate of 1.0 mm/s. In the C7 system, a 2.7 F OCT imaging catheter (Dragonfly, LightLab Imaging) was advanced distally to the lesion, and automatic pullback (at a rate of 20 mm/s) was initiated as soon as the blood was cleared by the injection of contrast media or dextran. All images were stored digitally for subsequent offline analysis.

OCT analysis

The OCT data were analysed using previously validated criteria for OCT plaque characterization.[16] Each plaque was classified as a fibrous plaque or lipid plaque. When lipids were present in ≥90° of any of the cross-sectional images within the plaque, it was considered a lipid-rich plaque. In the lipid-rich plaque, the maximum lipid arc was measured. Lipid length was defined as the length of the segment with a lipid arc of ≥90° within the plaque and measured on longitudinal view. The fibrous cap thickness of the lipid-rich plaque was measured three times at its thinnest part, and the average value was calculated. The presence of plaque rupture, TCFA, macrophage infiltration, microvessels, calcification, and intracoronary thrombi was estimated. Plaque rupture was defined as the presence of fibrous cap discontinuity with cavity formation in the plaque. TCFA was considered when the fibrous cap thickness was ≤65 μm in the lipid-rich plaque on a cross-sectional image. Macrophage infiltration was defined as bright spots with high OCT backscattering signal variances. A microvessel was defined as a no-signal tubular structure without a connection to the vessel lumen recognized on three or more consecutive cross-sectional images in the M2 system and two or more consecutive cross-sectional images in the C7 system. Intracoronary thrombus was defined as a mass (diameter ≥ 250 μm) protruding into the lumen of the artery. Calcification was defined as an area with a low backscatter signal and a sharp border inside a plaque. The OCT findings were analysed by two experienced observers who were blinded to the angiographic and clinical presentations using proprietary computer software (LightLab Imaging) after confirming proper calibration settings of the *Z*-offset. When there was any discordance between the observers,

a consensus reading was obtained. The intraclass correlation coefficients for inter- and intraobserver reliabilities of the fibrous cap thickness were 0.891 and 0.916, respectively.

Statistical analysis

Statistical analysis was performed using the JMP statistical software for Mac version 9.0.2 (SAS Institute, Inc., Cary, NC, USA). To analyse the HOMA-IR values as categorical variables, these levels were divided into tertiles: lower HOMA-IR (<1.40); middle HOMA-IR (1.40–2.50), and higher HOMA-IR (>2.50). Continuous variables were presented as mean ± standard deviation (SD); comparisons were performed using the one-way ANOVA and *post hoc* multiple comparison using Tukey–Kramer test or non-parametric Kruskal–Wallis test and *post hoc* multiple comparison using Steel–Dwass test for non-normally distributed variables. Categorical variables were presented as percentages and relative frequencies; comparisons were performed using the chi-square test, as appropriate. We performed simple linear regression analysis to determine the association between HOMA-IR values and thickness of fibrous cap. Levels of HOMA-IR did not distribute normally; therefore, transformed values of HOMA-IR in logarithm were used as variables for simple linear regression analysis. Univariate and multivariate logistic regression analyses were used to identify independent predictors of TCFA by adjusting for predefined variables. Several conventional and novel risk factors such as age, sex, ACS, body mass index (BMI), hypertension (HT), DM, HbA1c, LDL-cholesterol, statin use, high-sensitivity C-reactive protein (hs-C-reactive protein), and HOMA-IR were included in the multivariate model. A *P*-value <0.05 was considered statistically significant.

Results

Baseline characteristics

One hundred and fifty-five patients (68 ± 9 years, 114 men) were enrolled in this study. This study included 100 patients (65%) with SAP and 55 (35%) patients with ACS. One hundred patients (65%) had DM and the average HOMA-IR value was 2.38 ± 1.95 in this population. As described above, these subjects were divided into three groups according to tertiles (lower HOMA-IR, $n = 51$; middle HOMA-IR, $n = 52$; higher HOMA-IR, $n = 52$). The baseline characteristics of the three groups are shown in *Table 1*. There was no significant difference in the percentage of ACS among the three groups. There were no other significant clinical differences among the three groups except for the glucometabolic parameters, BMI, and triglyceride and LDL-cholesterol levels.

Table 1 Patient characteristics according to the HOMA-IR tertiles

	Lower tertile ($n = 51$)	Middle tertile ($n = 52$)	Higher tertile ($n = 52$)	*P*-value
Age, years	70 ± 9	66 ± 9	68 ± 9	0.14
Male sex, *n* (%)	39 (77)	38 (73)	37 (71)	0.83
ACS, *n* (%)	16 (31)	19 (37)	20 (39)	0.74
Previous PCI, *n* (%)	16 (31)	16 (31)	19 (37)	0.79
BMI, kg/mm^2	22.0 ± 3.1*	25.5 ± 3.6	25.6 ± 3.0	<0.0001
HT, *n* (%)	39 (77)	39 (75)	43 (83)	0.60
Current smoker, *n* (%)	33 (65)	29 (56)	33 (64)	0.60
DM, *n* (%)	28 (55)	33 (64)	39 (75)	0.10
Laboratory data				
eGFR, mL/min/1.73 m^2	60.9 ± 27.8*	66.1 ± 20.3	67.3 ± 21.8	0.34
hs-C-reactive protein, mg/L	1.6 ± 1.8	1.3 ± 1.3	1.3 ± 1.0	0.82
LDL-cholesterol, mg/dL	100 ± 25	119 ± 32*	104 ± 30	0.003
HDL-cholesterol, mg/dL	45 ± 13*	41 ± 12	40 ± 8	0.26
Triglycerides, mg/dL	107 ± 48*	151 ± 66	148 ± 54	<0.0001
Fasting glucose, mg/dL	96 ± 16*	108 ± 19*	117 ± 22	<0.0001
Fasting insulin, IU/L	4.1 ± 1.3*	7.2 ± 2.1*	15.7 ± 9.9	<0.0001
HOMA-IR	1.0 ± 0.3*	1.8 ± 0.3*	4.3 ± 2.3	<0.0001
HbA1c, %	6.4 ± 1.2*	6.7 ± 1.0	7.1 ± 1.4	0.04
Medication, *n* (%)				
Aspirin	33 (65)	42 (81)	39 (75)	0.17
ACE-I/ARB	21 (41)	25 (48)	33 (64)	0.07
Statin	30 (59)	30 (58)	30 (58)	0.99
Oral glycerides	17 (33)	21 (40)	23 (44)	0.52
Sulphonyl urea	12 (24	13 (25)	17 (33)	0.53

Values represent mean ± standard deviation or *n* (%).
ACS, acute coronary syndrome; BMI, body mass index; HT, hypertension; HOMA-IR, homeostasis model assessment of insulin resistance; PCI, percutaneous coronary intervention; eGFR, estimated glomerular filtration rate; hs-C-reactive protein, high-sensitivity C-reactive protein; LDL, low-density lipoprotein; HDL, high-density lipoprotein; HbA1c, haemoglobin HbA1c; ACE-I, angiotensin-converting enzyme inhibitor; ARB, angiotensin receptor blocker.
*$P < 0.05$ vs. patients in the higher tertile.

Angiographic results

The angiographic findings are summarized in *Table 2*. The distribution of culprit lesion location was similar among the three groups. The left anterior descending artery was the most frequent culprit lesion (46%), followed by the right coronary artery (39%) and the circumflex artery (15%). There were no significant differences in the frequency of multivessel disease and in the modified lesion classifications of the American College of Cardiology/American Heart Association. Based on quantitative coronary angiographic analysis, there were no statistical differences in the reference diameter, minimum lumen diameter, per cent diameter stenosis, and lesion length among the three groups.

Results of OCT analysis

In the present study, there was no significant difference in use percentage of the C7 system among the three groups (lower HOMA-IR: 37%; middle HOMA-IR: 37%; higher HOMA-IR: 48%; $P = 0.41$). *Table 3* and *Figure 1* show the OCT findings of the three groups. Patients in the higher HOMA-IR tertile had more frequent prevalence of lipid-rich plaques than those in the middle and lower tertiles (83 vs. 62 vs. 57%; $P = 0.01$), and lipid length was significantly longer in the higher HOMA-IR group than in the other two tertiles (vs. lower HOMA-IR, $P = 0.02$; vs. middle HOMA-IR, $P = 0.03$). The prevalence rates of TCFA among the higher, middle, and lower HOMA-IR tertiles were 50, 29, and 26% ($P = 0.02$). In addition, the microvessel prevalence rates among the higher, middle, and lower HOMA-IR tertiles were 54, 39, and 28% ($P = 0.02$). Furthermore, in the higher HOMA-IR group, the fibrous cap was significantly thinner than in the other two tertiles (vs. lower HOMA-IR, $P = 0.009$; vs. middle HOMA-IR, $P = 0.008$). The representative OCT images of the coronary culprit lesions in the lower HOMA-IR group and the higher HOMA-IR group are shown in *Figure 2*. Overall, there was a weak correlation between log HOMA-IR level

Table 2 Angiographic analysis of the HOMA-IR tertiles

	Lower tertile ($n = 51$)	Middle tertile ($n = 52$)	Higher tertile ($n = 52$)	*P*-value
Lesion location, *n* (%)				
Left anterior descending artery	23 (45)	27 (52)	21 (40)	0.65
Left circumflex artery	6 (12)	8 (15)	10 (19)	
Right coronary artery	22 (43)	17 (33)	21 (40)	
Multivessel disease	23 (45)	15 (29)	25 (48)	0.10
Modified ACC/AHA classification, *n* (%)				
B2/C lesion	35 (69)	43 (83)	39 (75)	0.25
Quantitative coronary analysis				
Reference diameter, mm	2.61 ± 0.48	2.78 ± 0.63	2.56 ± 0.49	0.09
Minimum lumen diameter, mm	0.87 ± 0.33	0.82 ± 0.32	0.85 ± 0.35	0.77
Diameter stenosis, %	66.4 ± 12.1	70.5 ± 9.4	67.1 ± 10.7	0.12
Lesion length, mm	16.5 ± 7.8	15.2 ± 5.9	17.1 ± 8.1	0.51

Values represent mean ± SD or *n* (%).
HOMA-IR, homeostasis model assessment of insulin resistance; ACC/AHA, American College of Cardiology/American Heart Association.

Table 3 OCT findings of the HOMA-IR tertiles

	Lower tertile ($n = 51$)	Middle tertile ($n = 52$)	Higher tertile ($n = 52$)	*P*-value
Minimal CSA, mm	1.6 ± 0.8	1.4 ± 0.8	1.5 ± 1.1	0.76
Lipid-rich plaque, *n* (%)	29 (57)	32 (62)	43 (83)	0.01
Calcification, *n* (%)	27 (53)	28 (54)	29 (56)	0.96
Thrombus, *n* (%)	7 (14)	14 (27)	13 (25)	0.22
Ruptured plaque, *n* (%)	8 (16)	6 (12)	8 (15)	0.80
Macrophage infiltration, *n* (%)	15 (29)	20 (39)	26 (50)	0.10
Microvessel, *n* (%)	14 (28)	20 (39)	28 (54)	0.02
TCFA, *n* (%)	13 (26)	15 (29)	26 (50)	0.02
Fibrous cap thickness, μm	95.5 ± 41.6*	89.0 ± 36.0*	69.7 ± 27.7	0.002
Lipid arc, degree	119 ± 111	124 ± 97	143 ± 81	0.32
Lipid length, mm	4.0 ± 5.2*	3.9 ± 4.1*	5.3 ± 3.7	0.04

Values represent mean ± SD or *n* (%).
OCT, optical coherence tomography; TCFA, thin-cap fibroatheroma; HOMA-IR, homeostasis model assessment of insulin resistance; CSA, cross-sectional area.
*$P < 0.05$ vs. patients in the higher tertile.

and fibrous cap thickness ($r = -0.251$, $P = 0.008$). In ACS, there was no significant correlation between log HOMA-IR and fibrous cap thickness ($r = -0.158$, $P = 0.25$), whereas log HOMA-IR significantly correlated with fibrous cap thickness in SAP ($r = -0.370$, $P = 0.004$) (*Figure 3*).

Predictors of TCFA presence

Univariate analysis showed that only two factors, including ACS [odds ratio (OR): 10.04; 95% confidence interval (CI): 4.76–22.2; $P < 0.0001$] and HOMA-IR >2.5 (OR: 2.68; 95% CI: 1.34–5.41; $P = 0.005$), significantly related to the presence of TCFA. After adjusting for age, gender, BMI, ACS, and several risk factors such as HT, DM, HbA1c, LDL-cholesterol, statin use, and hs-C-reactive protein, multivariate logistic regression analysis for predicting the presence of TCFA revealed that ACS (OR: 17.98; 95% CI: 7.12–52.02; $P < 0.0001$) and HOMA-IR >2.50 (OR: 3.57; 95% CI: 1.42–9.55; $P = 0.007$) were independent factors for predicting the presence of TCFA. However, DM was not significantly associated with TCFA (OR: 2.55; 95% CI: 0.76–9.10; $P = 0.13$) (*Table 4*).

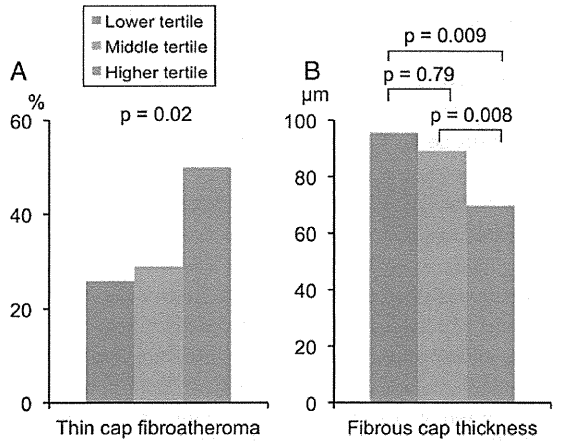

Figure 1 Comparison of the presence of TCFA and fibrous cap thickness as assessed by OCT among the three HOMA-IR tertiles. The TCFA prevalence rates of the higher, middle, and lower HOMA-IR tertiles were 50, 29, and 26%, respectively ($P = 0.02$). In the higher HOMA-IR group, the fibrous cap was significantly thinner than in the other two tertiles (vs. lower HOMA-IR, $P = 0.009$; vs. middle HOMA-IR, $P = 0.008$). TCFA, thin-cap fibroatheroma; OCT, optical coherence tomography; HOMA-IR, homeostasis model assessment of insulin resistance.

Discussion

The main findings of the present study were as follows: (i) patients in the higher HOMA-IR tertile had more frequent vulnerable plaque features such as lipid-rich plaque, TCFA, and microvessels as assessed by OCT than those in the middle and lower tertiles; in addition, the fibrous cap of patients in the higher IR tertile was significantly thinner than those in patients in the middle and lower tertiles; and (ii) higher HOMA-IR value (>2.50) predicted the presence of TCFA.

Several epidemiological studies have reported an association between insulin resistance and the prevalence of CAD. Amano *et al.*[12] demonstrated that IB-IVUS-derived lipid-rich plaque rates were significantly associated with higher HOMA-IR tertiles in 172 consecutive patients with both SAP and ACS. Our results are in accordance with their study. On the other hand, Mitsuhashi *et al.*[13] demonstrated that hyperinsulinaemia, defined as the calculated area under the insulin concentration–time curve, is associated with an increased lipid content measured by IB-IVUS and a greater plaque volume measured by conventional IVUS in non-culprit intermediate lesions in 82 non-diabetic patients with ACS, whereas there were no significant differences in the percentage of lipid area between the three HOMA-IR tertiles. We evaluated the lipid volume semi-quantitatively by measuring the presence of lipid-rich plaque, lipid arc, and length of the lipid-rich plaque due to the limited penetration depth of OCT. However, lipid-rich plaques

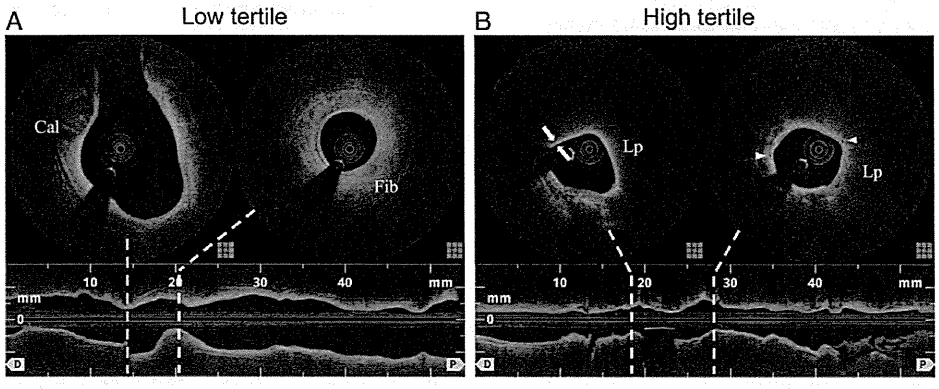

Figure 2 Representative OCT images of coronary culprit lesions. The OCT images were obtained from culprit lesions of the left anterior descending artery in stable angina patients with diabetes. (*A*) Fibrous (Fib) and calcified plaques (Cal) in the lower HOMA-IR tertile (0.41). (*B*) Lipid-rich plaques (Lp), including TCFA (thinnest fibrous cap thickness: 60 μm, white arrow) and microvessels (triangle arrow) in the higher HOMA-IR tertile (4.04). Abbreviations are as in *Figure 1*.